

Contents lists available at ScienceDirect

Journal of Rock Mechanics and Geotechnical Engineering

journal homepage: www.jrmge.cn



Full Length Article

Rheological behaviors of Na-montmorillonite considering particle interactions: A molecular dynamics study



Siqi Zhang ^{a, b}, Daoyuan Tan ^{a, *}, Honghu Zhu ^{a, **}, Huafu Pei ^c, Bin Shi ^a

- ^a School of Earth Sciences and Engineering, Nanjing University, Nanjing, 210023, China
- ^b Department of Civil and Environmental Engineering, The Hong Kong Polytechnic University, Hong Kong, 999077, China
- ^c School of Civil Engineering, State Key Lab of Coastal and Offshore Engineering, Dalian University of Technology, Dalian, 116026, China

ARTICLE INFO

Article history:
Received 26 April 2024
Received in revised form
23 June 2024
Accepted 15 July 2024
Available online 17 July 2024

Keywords:
Rheological behavior
Yield stress
Molecular dynamics
Particle interactions
Darjaguin-Landau-Verwey-Overbeek
(DLVO) theory
Microstructure
Montmorillonite suspension

ABSTRACT

Understanding the rheology of bentonite suspensions is crucial for ensuring the safety of engineering practices. However, the rheological mechanisms of bentonite remain unclear due to the limitations of conventional experimental techniques, particularly in assessing the microscopic interactions between clay particles and their impact on rheological properties. In this paper, the rheological behaviors of Namontmorillonite were studied with a focus on interparticle interactions. Both equilibrium molecular dynamics (MD) and non-equilibrium MD simulations were conducted to understand the physical properties of Na-montmorillonite under zero shear and various shear rates, respectively. The interaction between two parallel clay particles was determined in simulations, indicating that the classical Darjaguin-Landau-Verwey-Overbeek (DLVO) theory underestimates the interactions for a small separation distance. Na-montmorillonite exhibits a typical shear thinning behavior under shearing. However, as water content increases, it begins to behave more like liquid water. The yield stress of montmorillonite, as determined by the Bingham model, was found to be linearly related to the interaction pressures between clay particles. Besides MD simulations, the microstructure of clay suspension was further quantified using the separation distance and incline angle between non-parallel clay particles. Based on MD results and the quantified clay structure, a model was developed to estimate the yield stress of montmorillonite considering various influence factors, including electrolyte concentration, temperature, and solid fraction. Finally, from a comparison with calculated and experimental data, the results confirm the good performance of the proposed model. These findings provide significant insights for understanding the rheological soil behaviors and evaluating the yield stress of bentonite suspensions.

© 2025 Institute of Rock and Soil Mechanics, Chinese Academy of Sciences. Published by Elsevier B.V. This is an open access article under the CC BY-NC-ND license (http://creativecommons.org/licenses/by-nc-nd/4.0/).

1. Introduction

Bentonites, primarily composed of montmorillonite, are commonly used in various fields such as civil and drilling engineering, medicine, and industry due to their unique properties, including high surface area, large cations exchange capacity, high swelling capacity, and low permeability (Komine and Ogata, 2004; Holmboe and Bourg, 2014; Neuzil, 2019). The rheology of bentonite has a close relation with long-term safety in geotechnical

E-mail addresses: dytan@nju.edu.cn (D. Tan), zhh@nju.edu.cn (H. Zhu).

Peer review under responsibility of Institute of Rock and Soil Mechanics, Chinese Academy of Sciences.

engineering (Liingaard et al., 2004; Feng et al., 2017; Xie et al., 2023). For instance, its rheological properties have gained much attention from researchers and engineers involved in the design of nuclear waste disposal (Gijven, 1990; Chegbeleh et al., 2014). Bentonite suspensions are also treated as drilling and retaining fluids to protect the borehole walls due to their special rheological properties, including the shear thinning behavior and high yield stress (Laribi et al., 2005). The rheological behaviors make them suitable for use as slurries in the slurry shield tunneling method for submarine tunnel construction (Wang et al., 2022; Zhao et al., 2024). Furthermore, the rheology of fine-grained soil is crucial for the formation and characteristics of debris flows (Jeong et al., 2012; Abraham et al., 2022). Therefore, it is of great importance to investigate the interaction of clay particles in aqueous solution to gain an understanding of the rheological behavior of

^{*} Corresponding author.

^{**} Corresponding author.

montmorillonite-water systems.

Researches have been extensively conducted on the rheological behaviors of bentonite suspensions (e.g. Avery and Ramsay, 1986; Luckham and Rossi, 1999; Durán et al., 2000; Kök et al., 2000; Laribi et al., 2005). Various influence factors, such as pH value (Benna et al., 1999), electrolytes (Brandenburg and Lagaly, 1988), temperature (Ren et al., 2021; Salih, 2022), ionic strength (Ramos-Tejada et al., 2001), and additives (Günister et al., 2006; Yoon and El Mohtar, 2015), have been examined in experimental studies. It is recognized that the rheology of clay suspension is strongly associated with the interparticle interactions between clay particles (Laxton and Berg, 2006; Lin et al., 2015; Du et al., 2020). In the classical Darjaguin-Landau-Verwey-Overbeek (DLVO) theory, interparticle interaction of clay particles contains van der Waals forces and electrical double layer (EDL) forces, which has been used to successfully describe the swelling and compressive properties of clay (Sridharan and Choudhury, 2002; Abdurrahmanoglu and Okay, 2010; Anandarajah and Amarasinghe, 2013; Yan and Zhang, 2021). Previous literature primarily focuses on the relationship between particle interactions and the rheological behaviors of clay, as well as the influence of the micro-structure of clay, as illustrated in Fig. 1. The most important rheological parameter is the yield stress that reflects the existence of the network and the strength of particle interactions in clay suspension. Sakairi et al. (2005) proposed an equation to estimate the yield stress of montmorillonite based on the DLVO theory, and it assumes that the yield stress equals the EDL repulsive pressure. Scholars have also explored the relationship between yield stress and colloidal properties (such as zeta potential) of clay suspensions (Laxton and Berg, 2006; Teh et al., 2009). Leong (2024) provided direct evidence that attributes the timedependent behavior of clay to the EDL repulsive force. Furthermore, unlike simple colloidal solutions, clay suspensions possess complex microstructures, including Face-Face (F-F), Edge-Face (E-F), and Edge-Edge (E-E) arrangements, which significantly influence the rheological behaviors of clay. Lin et al. (2015) introduced a fitting parameter to the DLVO theory to represent the clay structure and calculate the yield stress of kaolin suspensions. Deng et al. (2023) estimated the yield stress of bentonite suspensions with varying solid concentrations by considering the inclination angle and separation distribution between clay particles. Although the DLVO-based estimation of yield stress demonstrated acceptable consistency with published experimental data, several challenges still need to be addressed. Firstly, the relationship between yield stress and particle interactions requires further verification. Secondly, simplification of the particle interaction function based on the DLVO theory is necessary for ease of use. Finally, the microstructure of clay suspensions with changing solid fractions should be taken into account.

The macroscopic rheological behavior is strongly influenced by the microscopic interactions between colloidal particles (Gupta et al., 2011; Deng et al., 2023). Over the past decades, the rheological properties of clay suspensions have been primarily investigated through experimental techniques such as rheometry, viscoelastic measurements, and oscillatory experiments (Luckham and Rossi, 1999; Landrou et al., 2018; Yoshida et al., 2018, 2022). However, quantitatively determining interparticle interactions at the nanoscale poses challenges due to experimental limitations in size. Additionally, due to the complex microstructure of clay gels, explaining the rheological mechanisms in terms of microscopic interactions has proven to be elusive. With advancements in computing technology, non-equilibrium molecular dynamics (NEMD) has emerged as a successful approach for studying the rheology of colloidal gels at the nanoscale (Kröger and Hess, 2000; Jabbarzadeh and Tanner, 2006; Dickinson, 2013). For example, NEMD simulations have been employed to investigate the rheological behaviors of thin liquid films and nanoconfined water (Jabbarzadeh et al., 1997; Kapoor et al., 2014). Xu et al. (2015) utilized MD simulations to investigate the rheology of clay nanocomposite hydrogels. Pisarev and Kalinichev (2022) simulated the shear flow of pentane in pyrophyllite and montmorillonite nanopores by NEMD and calculated the viscosity-density and viscositypressure relationships of the pentane-clay system. Some other scholars have also explored the impact of shear rate on the friction behaviors of soil-water systems using MD simulations (e.g. Xu et al., 2023; Wei et al., 2024). Molecular dynamics simulations have shown promising results in predicting the atomic-scale structure and physical behaviors of clay, leading to significant advancements in the study of swelling, colloidal, and transport properties of montmorillonite (Katti et al., 2018; Pei and Zhang, 2021; Zhang et al., 2022; Du et al., 2023; Meng et al., 2023). MD has also been

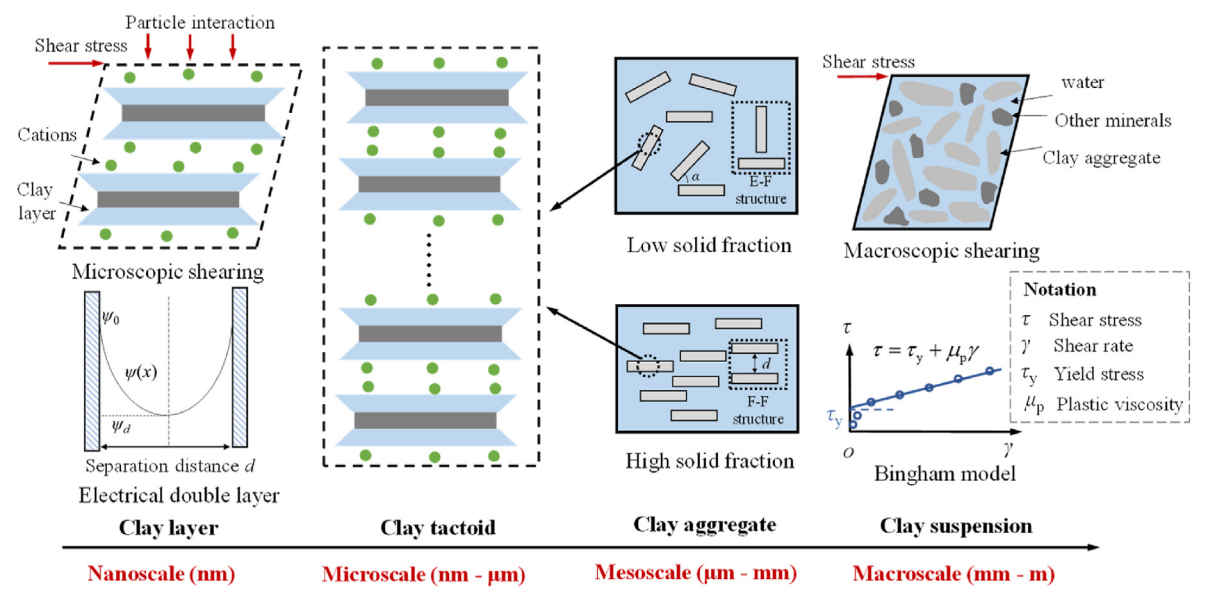


Fig. 1. Micro-structure of clay suspension and the relationship between particle interaction and rheological behaviors of clay.

used to determine the interparticle interactions of clay particles (Hsiao and Hedstrom, 2017). Consequently, employing MD methods enables the determination of the interparticle interactions and helps elucidate the rheological behaviors of clay by eliminating the complexities associated with the complex structure of clay systems.

Building upon previous researches, this paper investigates the rheological behavior of Na-montmorillonite through the utilization of MD simulations. The interactions between montmorillonite layers were calculated, allowing for a comprehensive study of the rheological characteristics of Na-montmorillonite, including the viscosity-shear rate relationship and yield stress. Subsequently, based on the insights gained from the MD simulations, a function was developed to predict the yield stress considering the microstructure of the clay suspension. Furthermore, the proposed model was employed to estimate the impact of various factors, such as solid fraction, electrolyte concentration, and temperature, on the yield stress of bentonite. To elucidate the logical flow of this paper, a flowchart illustrating the study on the rheology of Namontmorillonite is presented in Fig. 2.

2. Simulation methodology

This study investigates the rheological properties of two parallel Na-montmorillonite particles. An Arizona-type montmorillonite model with a unit cell formula of $Na_{0.75}^+Si_8(Al_{3.25}Mg_{0.75})O_{20}(OH)_4$ was utilized, which was constructed based on a pyrophyllite unit cell structure obtained through single-crystal X-ray refinement (Lee and Guggenheim, 1981). To represent a clay particle, a single crystal with a 4×4 unit cell (extending 2.06 nm and 3.58 nm in x-and y-direction, respectively; 1 nm = 1×10^{-9} m) was constructed. Within the clay layer, Mg/Al isomorphous substitutions followed

Lowenstein's substitute rule, which is distributed throughout the octahedral sheet. These substitutions lead to charge deficiencies on the surface, which contributes to the electronegativity of clay particles. To investigate the influence of charge density on the physical properties of montmorillonite, three types of clay particles were constructed. These particles contained 6, 8, and 12 substitutions within the crystal structure, resulting in surface charge densities of -0.065, -0.086, and -0.13C/m², respectively. The two parallel clay particles with the same surface charge density formed a slit pore, and pore widths of 1 nm, 2 nm, 3 nm, 4 nm, and 5 nm were selected to examine the tendency of rheological behavior of the water-clay system with varying separation distances. The pore width was determined as the distance between the nearest oxygen atoms in two separate clay sheets. To model the montmorillonitewater system in the saturated state, the pore was filled with water molecules at a bulk density of 0.997 g/cm³. In the initial configurations, Na⁺ cations were randomly distributed within the nanopore and the other side of the clay particles to maintain charge balance. All the molecules in the pore were prepared using the Packmol package (Martínez et al., 2009) to gain a good initial configuration. Periodic boundaries were set in all directions. To get an equilibrium configuration, the clay model was relaxed with the micro-canonical (NVE) ensemble for 0.5 ns (1 ns = 1×10^{-9} s), followed by the canonical (NVT) ensemble for 1 ns, and then for 2 ns in the isothermal-isobaric (NPT) ensemble. This equilibrium process in different ensembles in the sequence is consistent with previous literature (e.g. Wei et al., 2022; Du et al., 2023; Li et al., 2024). The Nose-Hoover thermostat and barostat were used to control the environmental condition of the system at a temperature of 298 K and 1 standard atmospheric pressure. The separation distance was allowed to adjust during the simulation, resulting in a slightly different value from the predetermined width after

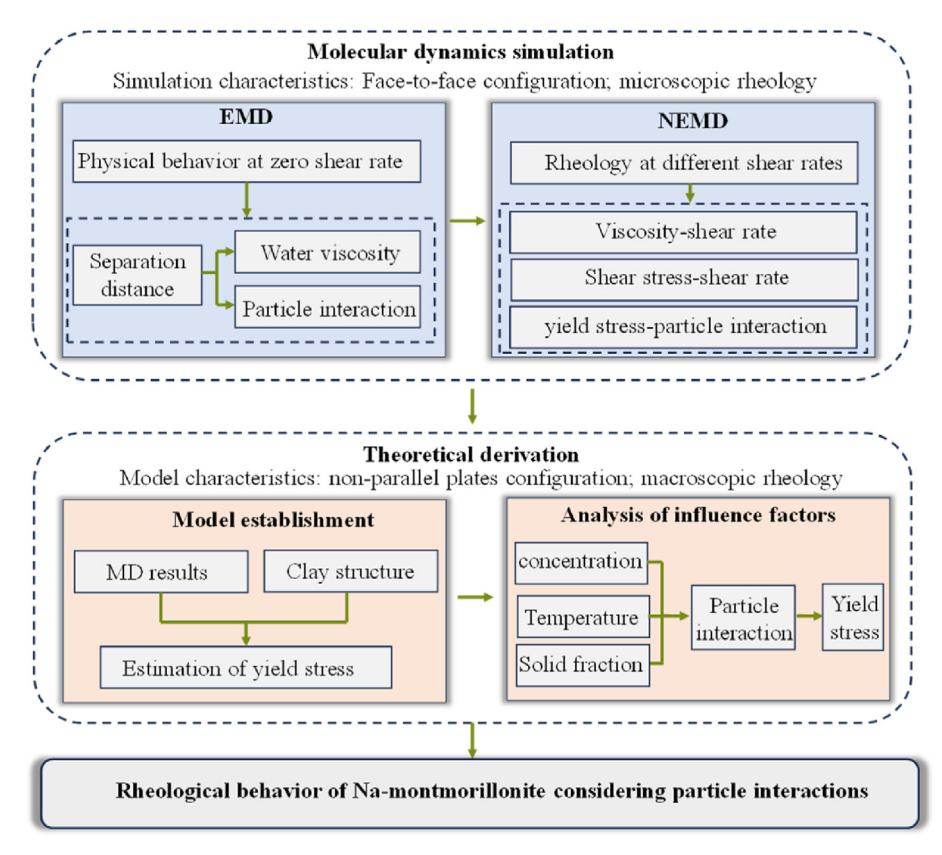


Fig. 2. A flowchart of studying the rheology of Na-montmorillonite.

relaxation. After relaxation, the boundary condition in *z*-direction was changed to a fixed boundary. Vacuum layers with a thickness of 2 nm were added above and below the clay model to mitigate boundary effects. A snapshot of the Na-montmorillonite pore model with 433 water molecules is shown in Fig. 3.

After the modeling process, equilibrium molecular dynamics (EMD) simulations were performed to investigate the physical properties of Na-montmorillonite under a zero-shear condition. Each model was simulated by performing 10 ns MD runs in the NVT ensemble under 298 K temperature. The lower clay particle was fixed in all directions throughout the simulation. Potential energy and atomic trajectories were recorded at intervals of 1 ps (1 ps = $1\,\times\,10^{-12}$ s). The self-diffusion coefficient and viscosity of water molecules within the pore were calculated, along with the determination of the density distribution of cations within the nanopore. Then, NEMD simulations were performed to explore the rheological behavior of the montmorillonite-water system. In these simulations, the movement of clay layers was integrated under the NVE ensemble. Then, the upper clay layer was subjected to a constant velocity in y-direction, while the lower layer remained fixed, resulting in a shear process within yz plane. A Langevin thermostat was applied to the water molecules and Na⁺ cations in the pore to achieve the desired temperature. The shear process generated a Couette flow in y-direction within the nanopore. The thermostat used in the NEMD simulations was only coupled to degrees of freedom perpendicular to the flow direction. Furthermore, the temperature of interlayer species was calculated by subtracting the ramped velocity profile of the Couette flow. A wide shear rate range of $10^{-7} \le \gamma \le 10 \text{ ps}^{-1}$ was considered in the simulations by applying different velocities to the upper layer. It is worth noting that the chosen shear rate is higher than that used in experiments, but it falls within the commonly employed range in NEMD simulations for rheological studies (Jabbarzadeh and Tanner, 2006; Dickinson, 2013; Xu et al., 2023). The aim of the high shear rate is to avoid excessive noise and obtain reasonable accuracy. The duration of the simulations depended on the size of the model, and a maximum simulation time of 30 ns was found to be sufficient to obtain reliable outcomes in this study.

In this paper, the clay-clay interactions and clay-water interactions in the model systems were defined by the ClayFF force field (Cygan et al., 2004). The extended simple point charge (SPC/E) water model was utilized to calculate the water-water interactions. Water molecules were kept rigid during the simulation by the SHAKE algorithm. The Lennard Jones interactions were truncated to 1.25 nm and the Coulomb interactions were calculated by the PPPM

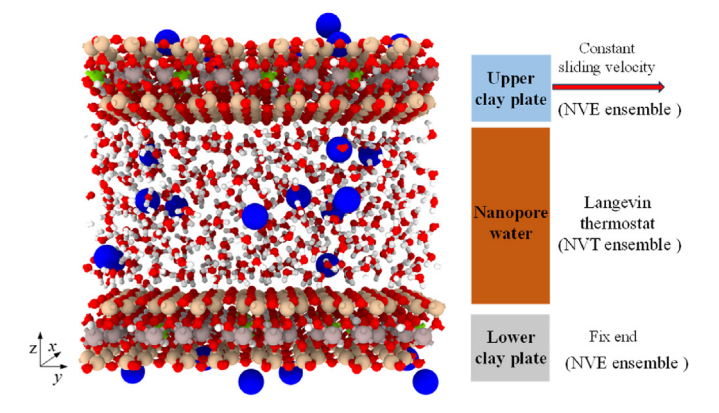


Fig. 3. Snapshot of a Na-montmorillonite pore model with a separation distance of 2.03 nm, containing 433 water molecules. Atoms are colored as follows: Na, blue; H, white; O, red; Si, yellow; Mg, green; Al, pinkish gray.

method with 99.99% accuracy. The time step of the simulation was set as 1 fs (1 fs = 1×10^{-15} s) for integration of Newton's motion equation, while the time step was decreased to 0.5 fs for cases of high shear rate ($\gamma \geq 10^{-2}~\text{ps}^{-1}$). All MD simulations were performed by using the LAMMPS package (Plimpton, 1995). Before simulating, the choice of the slit pore model of montmorillonite used in the study was explained:

- (1) The plate-like montmorillonite particles facilitate the formation of face-to-face aligned particle clusters, driven by the principle of energy minimization. Thus, the slit-shaped pore plays a major role in the pore structure montmorillonite suspension. Within these pores, intricate microscopic interactions occur among clay-clay, clay-water, and watercation interfaces, leading to complex physicochemical changes. These microscopic interactions have a profound influence on the macroscopic mechanical behavior of clay. Consequently, researchers have incorporated nanoscale interface phenomena of constituent mineral crystals into classical models, aiming to better describe the macroscopic behaviors of clay (Kyokawa, 2021; Meng et al., 2023).
- (2) The model in this study simulated the sliding friction between parallel plates. The presence of plate-like montmorillonite particles and the formation of slit pores significantly contribute to the friction behavior, which plays a major role in the shear mechanism of montmorillonite. Hattab et al. (2015) utilized scanning electron microscopy (SEM) to examine the microstructure during the shearing of a kaolinite/montmorillonite clay mixture. They observed the formation of face-to-face aligned particle clusters, primarily within the montmorillonite component, where the sliding mechanism is activated. Similarly, Wei et al. (2024) acknowledged that frictional sliding between clay particles governs the microscopic behavior of clay deformation failure. Furthermore, Ying et al. (2024) established a numerical correlation between the macroscopic friction angle of montmorillonite and the microscopic friction coefficient between two parallel particles through MD simulations. Consequently, simulating the friction process between parallel clay plates has become a common approach in MD simulations for studying the shear mechanism of clay.
- (3) Due to the limitations in computational efficiency, the commonly used molecular models are limited to nanoscale dimensions. Scholars have constructed slit pores with widths ranging from 1 nm to 7.5 nm to investigate the microscopic behaviors of Na-montmorillonite, including seepage (Zhang et al., 2022), friction (Ying et al., 2024), and water adsorption behaviors (Zhang and Pei, 2021). The slit pore model has also been employed to determine the structure of the electrical double layer (Bourg and Sposito, 2011; Pei and Zhang, 2021) and calculate particle interactions (Amarasinghe and Anandarajah, 2013). Therefore, this model provides a sufficiently large representation to study the microscopic behaviors of the clay-water system.

3. Physical behaviors of montmorillonite at zero shear condition

3.1. Self-diffusion and viscosity of water in clay pore

As the mobility of pore water plays a major role in the viscosity of the clay-water system, the self-diffusion and viscosity of water were determined in this study. Self-diffusion coefficients of water molecules characterize the mobility of water confined in the clay

nanopore, which can be determined by the Einstein relation (Li et al., 2019):

$$D = \lim_{t \to \infty} \frac{\frac{1}{N} \sum_{i=1}^{N} \langle |r_i(t) - r_i(t_0)|^2 \rangle}{2nt} = \lim_{t \to \infty} \frac{MSD(t)}{2nt}$$
(1)

where MSD (the mean squared displacement) is the numerator of the equation, which is defined as the displacement summation of N number atoms from time t_0 to time t; $r_i(t)$ is the coordinates of atom i at time t; n is the order of dimension equal to 1, 2, or 3 for the one-, two-, and three-dimensional (1D, 2D, and 3D) diffusion coefficients, respectively.

In the paper, we calculated 2D (in *xy* plane) and 3D diffusion coefficients to compare the mobility of water molecules in the nanopore with different separation distances. The shear viscosity of interlayer water molecules was obtained from EMD simulations in the NVT ensemble by two methods. First, a standard Green-Kubo equation on the autocorrelation function of the stress tensor elements was used (Yeh and Hummer, 2004):

$$\eta = \frac{1}{5} \sum_{\alpha,\beta} \lim_{t \to \infty} \frac{V}{k_B T} \int \langle p_{\alpha\beta}(t) p_{\alpha\beta}(0) \rangle dt$$
 (2)

where η is the shear viscosity; V is the volume of interlayer space; k_B is the Boltzmann coefficient; T is the temperature; $p_{\alpha\beta}$ is the parameter of five anisotropic components of the stress tensor including p_{Xy} , p_{XZ} , p_{YZ} , $(p_{XX}-p_{YY})/2$ and $(p_{YY}-p_{ZZ})/2$. The stress tensor elements were recorded every 5 fs and a suitable integration time t was found to be 4 ps in this study. Second, the viscosity of water molecules in the interlayer space can be estimated based on the Stokes-Einstein relation that the viscosity has a linear relationship with the reciprocal of the self-diffusion coefficient (Zhang and Pei, 2021):

$$\eta_{\rm int} = \eta_{\rm bulk} \frac{D_{\rm bulk}}{D_{\rm int}} \tag{3}$$

where η_{bulk} and D_{bulk} are the viscosity and self-diffusion coefficient of bulk SPC/E water, respectively; D_{int} is the self-diffusion coefficient of water confined in clay pore.

Fig. 4a illustrates the 2D (in xy plane, D_{xy}) and 3D self-diffusion coefficients (D_{xyz}) of water molecules in the nanopore. It is evident that the mobility of water confined within the clay pore is lower compared to bulk water. The self-diffusion coefficient of bulk SPC/E water (D_{bulk}) in this study is determined to be (26.17 ± 0.02) × 10^{-10} m²/s, which is close to the value of (26.8 ± 0.03) × 10^{-10} m²/s reported by Holmboe and Bourg (2014). When the separation distance between two clay plates exceeds 4 nm, the value of D_{xy} is close to D_{bulk} ; however, D_{xyz} remains 33% smaller than that of bulk water. It implies that water molecules are more restricted in the direction perpendicular to the clay surface. In general, the surface charge density of montmorillonite has little difference in the diffusion of water molecules. However, the diffusion coefficient decreases with increasing charge density at the smallest separation distance (around 1 nm).

The viscosity of water molecules in the clay pore was also calculated using the Green-Kubo equation (Eq. (2)) and the Stokes-Einstein relation (Eq. (3)), as presented in Table 1. Notably, D_{xyz} was utilized in Eq. (3) to estimate the viscosity. The values obtained by Eq. (2) closely align with those derived from Eq. (3). The viscosity of pore water increases exponentially as the pore size decreases. Low (1976) measured interlayer water viscosity in Wyoming-type Namontmorillonite as a function of the interlayer distance at 298 K using a combined method involving viscous flow at different temperatures, the self-diffusion method, and neutron scattering. The comparison between simulation and experimental data is illustrated in Fig. 4b. The viscosity of SPC/E water in the bulk solution was determined to be (0.686 + 0.013) mPa s, which is consistent with other simulation results of (0.66 + 0.08) mPa s (e.g. Balasubramanian et al., 1996; Mark and Nilsson, 2001). However, these values underestimated the experimental result of 0.89 mPa s for the viscosity of bulk water. To facilitate a better comparison, the simulation and experimental data were normalized by the viscosity of bulk SPC/E water and bulk water, respectively. It can be observed that the simulation results show a good agreement with the experimental data, demonstrating the good accuracy of MD simulations in the paper. In clay with lower charge densities, water molecules experience relatively higher mobility and lower viscosity due to fewer cations impeding their movement. However, this effect is only pronounced in small-sized pores.

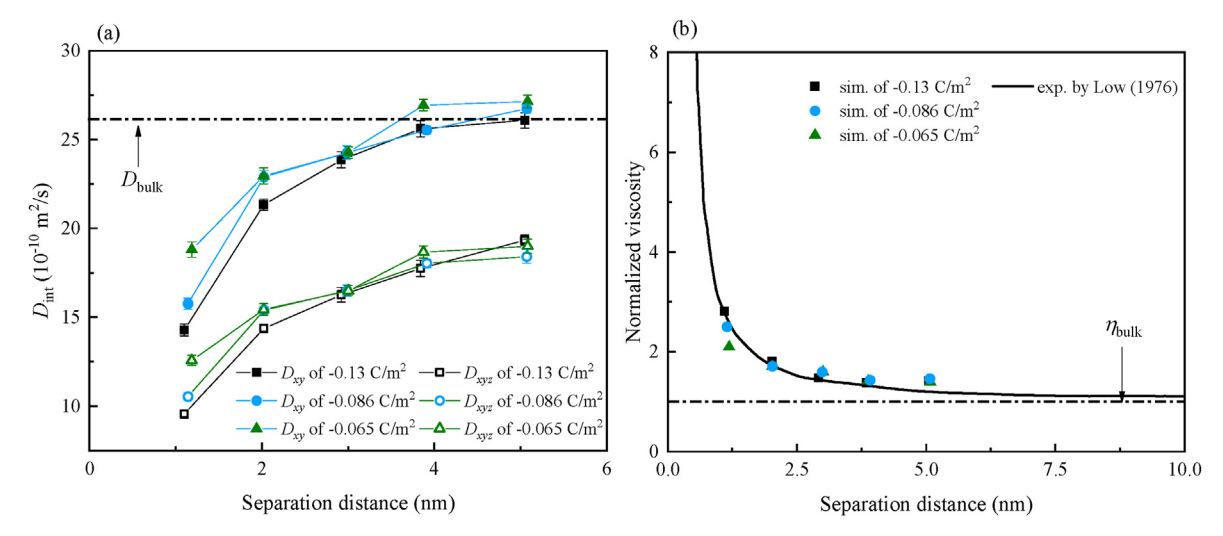


Fig. 4. (a) Two- and three-dimensional self-diffusion coefficients of water molecules in the Na-montmorillonite pore, and (b) The normalized viscosity of water in pores as a function of separation distance for clay with different charge densities in MD simulations, compared with experimental data by Low (1976).

Table 1 The two-dimensional self-coefficients (D_{xy}) and viscosity (η_{int}) of water molecules in pores of Na-montmorillonite with a surface charge of -0.13 C/m².

Separation distance (nm)	Number of water molecules in the pore	$D_{xy} (10^{-10} \text{ m}^2/\text{s})$	η _{int} (mPa s)	
			Eq. (2)	Eq. (3)
1.11	205	14.28 ± 0.03	1.91	1.86
2.03	433	21.33 ± 0.03	1.22	1.24
2.95	661	23.86 ± 0.05	1.00	1.09
3.87	889	25.60 ± 0.04	0.96	1.00
5.09	1187	27.48 ± 0.04	0.93	0.92

3.2. Interaction between clay particles

The interaction between two parallel clay particles can be evaluated based on the DLVO theory. This interaction P encompasses the attractive van der Waals pressure $P_{\rm vdW}$ and the repulsive EDL pressure $P_{\rm edl}$.

$$P = P_{\text{vdW}} + P_{\text{edl}} \tag{4}$$

For two parallel particles with the thickness h separated by a separation distance d, the van der Waals pressure, P_{vdW} , is given by (Hsiao and Hedstrom, 2017):

$$P_{\text{vdW}} = -\frac{A_{\text{H}}}{6\pi} \left[\frac{1}{d^3} + \frac{1}{(d+2h)^3} - \frac{2}{(d+h)^3} \right]$$
 (5)

where $A_{\rm H}$ is the Hamaker constant and is assumed to be 2.2×10^{-20} J in this study, as suggested by Zhang and Lu (2018). The EDL repulsion can be calculated by the well-known Gouy-Chapman model:

$$-\kappa \frac{d}{2} = \int_{\phi_0}^{\phi_{\text{mid}}} (2\cosh y - 2\cosh \phi_{\text{mid}})^{-1/2} dy$$

$$\sigma = \sqrt{2D_r c^0 k_B T} (2\cosh \phi_0 - 2\cosh \phi_{\text{mid}})^{1/2}$$

$$\kappa = \sqrt{\frac{2c^0 e'^2 v^2}{D_r k_B T}}$$

$$P_{\text{edl}} = 2c^0 k_B T (\cosh \phi_{\text{mid}} - 1)$$

$$(6)$$

where c^0 is the number concentration of cations in the equilibrium solution; v is the valence of the cation; σ is the surface charge density; e' is the elementary electric charge; $k_{\rm B}$ is the Boltzmann constant; κ (m $^{-1}$) is the reciprocal of the Debye length; $D_{\rm r}$ is the relative dielectric constant; Φ_0 and $\Phi_{\rm mid}$ are the dimensionless electrical potential at the clay surface and the potential at the midplane, respectively.

By combining Eqs. (4)–(6), the interaction between two parallel clay particles can be calculated, which the above is the DLVO theory. However, previous studies (e.g. Hsiao and Hedstrom, 2017; Shen and Bourg, 2021; Pei and Zhang, 2021; Zhang and Pei, 2021) have demonstrated the limitations of the Gouy-Chapman model in accurately describing the distribution of cations within clay pores and in predicting the EDL pressure for short separations between two parallel plates. Besides, the difficulty in calculating the EDL force based on Eq. (6) limits the application of the DLVO theory. In essence, the EDL repulsion arises from the difference in ionic concentrations between the mid-plane and the bulk solution (Sridharan and Jayadeva, 1982):

$$P_{\rm edl} = k_{\rm B} T c^0 \left(\frac{c_{\rm mid}}{c^0} + \frac{c^0}{c_{\rm mid}} - 2 \right) \tag{7}$$

where $c_{\rm mid}$ is the concentration of cations at the mid-plane in the clay pore.

The density profiles of cations within the nanopore can be obtained through MD simulations, allowing for calculation of the concentration at the mid-plane. Consequently, the EDL repulsion can be easily determined by using Eq. (7) through MD simulation. Previous experiments (e.g. Bolt, 1956; Komine and Ogata, 2004) showed that the concentration of ions in pore water of bentonite ranges from 10^{-2} mol/L to 10^{-1} mol/L. In this study, the concentration in the bulk solution took the average value of experimental data as 0.05 mol/L.

The concentration distributions of Na⁺ within the montmorillonite pore are depicted in Fig. 5a. It is evident that the Na⁺ concentration exponentially diminishes as one moves away from the clay surface, reaching a minimum value at the mid-plane of the pore. Fig. 5b shows the Na⁺ concentration at the mid-plane with the separation distance for montmorillonite of various charge densities. The Na⁺ concentration at the mid-plane decreases rapidly as the separation distance increases. As the charge density decreases, the mid-plane concentration reduces due to a lower number of cations in the pore. However, this difference becomes less pronounced as the separation distance increases.

By combining Eqs. (4), (5) and (7), the interaction between two parallel clay particles at different separations can be calculated once the concentration at the mid-plane is determined. Moreover, the interaction between the particles was also computed using the classical DLVO theory (see Eqs. (4)—(6)), as illustrated in Fig. 6a. The predicted values by the DLVO theory match closely with the simulation data when the separation distance exceeds 4 nm. However, as the distance decreases, the predictions begin to underestimate the repulsive interaction. This finding is consistent with other investigations (e.g. Hsiao and Hedstrom, 2017; Shen and Bourg, 2021). As described by Heimenz (1986), the repulsive force of two plates based on the Gouy-Chapman model can be simplified as follows:

$$P_{\rm edl} = 64c^0 k_{\rm B} T \tanh^2 \left(\frac{\Phi_0}{4}\right) \exp(-\kappa d) \tag{8}$$

It shows that the EDL force has an exponential function of κd when the surface potential Φ_0 is constant. Liu et al. (2020) demonstrated that the surface potential is unchanged after a quick reduction with the separation distance increases. Therefore, the value of $\tanh^2(\frac{\phi_0}{4})$ was considered as a constant value. As shown in Fig. 6a, Eq. (8) is in good agreement with MD simulations with the fitting parameters of Φ_0 and κ . The fitted κ is 0.8 m⁻¹, which is close to the value of 0.74 m⁻¹ for 0.05 mol/L solutions. In addition, the surface potential is fitted as -90.9 mV, falling into the range of -150 mV and -75 mV for montmorillonite in experiments and other simulations (e.g. Hou et al., 2009; Zhang and Pei, 2021). Therefore, MD shows that Eq. (8) can be used to calculate the EDL repulsion and thereby calculate the particle interactions by incorporating Eq. (5). Particle interactions for different charge densities are shown in Fig. 6b. Eq. (8) can well fit the interaction pressure for

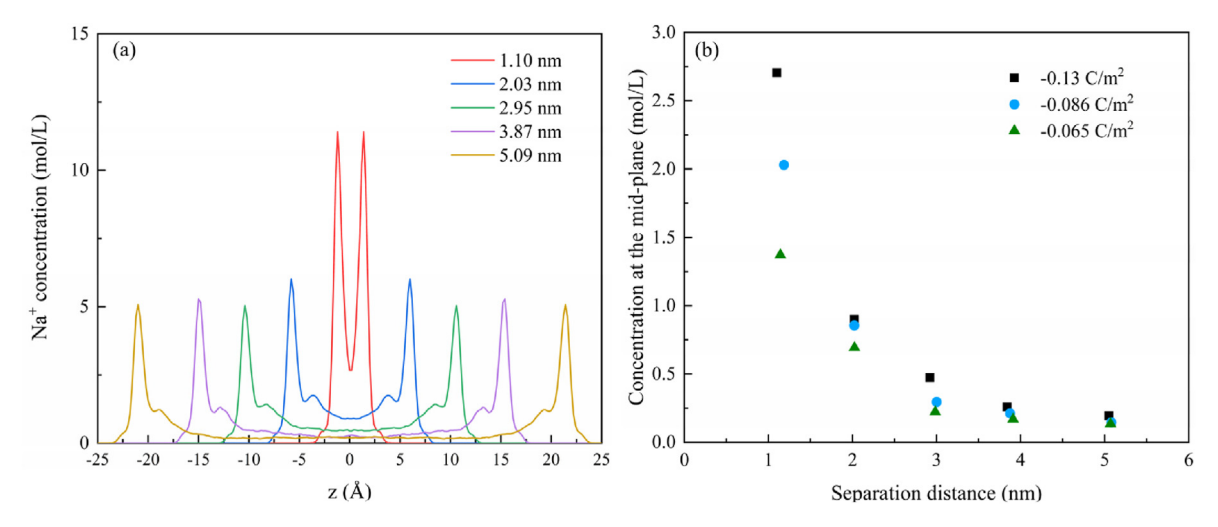


Fig. 5. (a) Density profiles of Na⁺ in the pore of montmorillonite with $\sigma=-0.13$ C/m² for different pore sizes, and (b) Na⁺ concentration at the mid-plane with the separation distance for montmorillonite of various charge densities. 1 Å = 1×10^{-10} m.

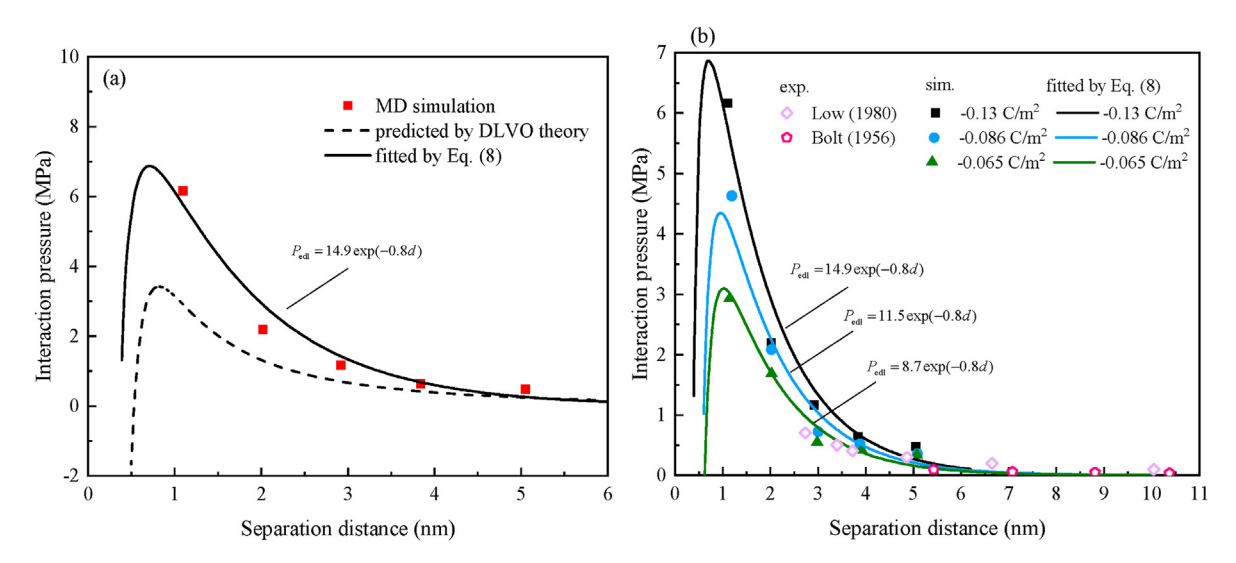


Fig. 6. (a) Interaction pressure of two parallel Na-montmorillonite particles with $\sigma = -0.13 \text{ C/m}^2$ as a function of the separation distance calculated by MD simulations, DLVO theory, and fitted by Eq. (8), respectively; and (b) interaction pressure for different surface charge densities calculated by MD simulations and fitted by Eq. (8), with comparison of experimental results.

all cases. The fitted values of κ are the same for three types of montmorillonites but only change in the fitted value of Φ_0 . As shown in Eq. (6), the surface potential Φ_0 is related to surface charge density, which further proves the rationality and applicability of Eq. (8). When the separation distance exceeds 3 nm, the interaction pressure for different charge densities converges. Consequently, the influence of surface charge density is typically disregarded in the calculation of the clay particle interactions based on the DLVO theory, primarily due to the large pores within the clay structure (Sridharan and Choudhury, 2002; Deng et al., 2023). Notably, Bolt (1956) and Low (1980) conducted studies on Namontmorillonite, measuring the effective stress as a function of separation distance. The effective stress is commonly attributed to the interaction between clay particles according to the DLVO theory (Sridharan and Jayadeva, 1982; Sridharan and Choudhury, 2002; Anandarajah and Amarasinghe, 2013). Comparing our simulation data with experimental data reveals a close agreement, confirming the accuracy of our simulations.

4. Rheology of Na-montmorillonite

4.1. Rheological behaviors

The rheological behaviors of Na-montmorillonite-water systems were investigated using NEMD simulations. During the simulation, a typical Couette flow was observed within the clay nanopore, as evidenced by the velocity profile of water molecules depicted in Fig. 7. The presence of shear flow in the pore water confirms the continuous shear process between the two clay particles throughout the simulation. Fig. 8a illustrates the shear stress of the Na-montmorillonite layer with a separation distance of 2.03 nm under various shear rates, changing with the simulation time. The values converge after a simulation time of 5 ns, indicating sufficient time for obtaining accurate results in this study. It can be observed that the shear stress increases with increasing shear rate. Furthermore, Fig. 8b illustrates the variation in separation distance at different shear rates. Under low shear rates, the separation distance

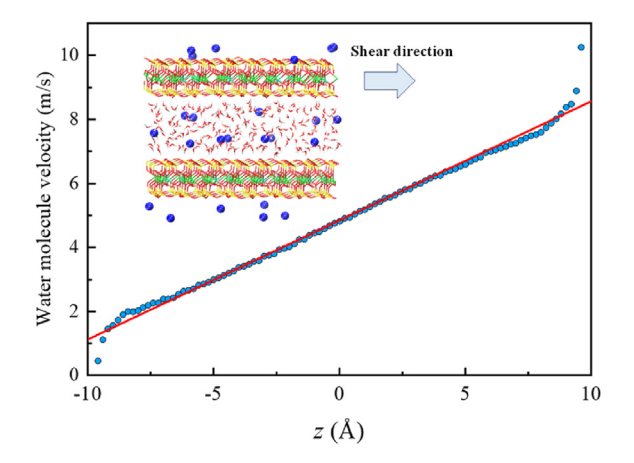


Fig. 7. Velocity of water molecules in 2.03 nm pore of Na-montmorillonite with a -0.13 C/m² charge density under the shear rate of 2.45×10^{-2} ps⁻¹. The red line is fitted by water velocity. z is the direction along the pore width. $1 \text{ Å} = 1 \times 10^{-10}$ m.

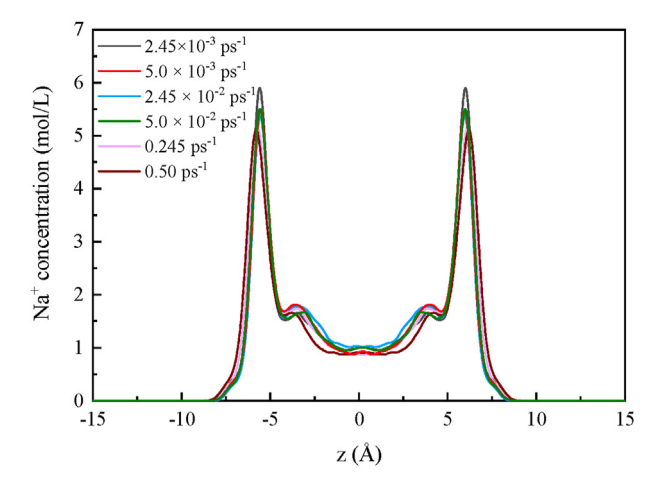


Fig. 9. Density profiles of Na⁺ in the 2.03 nm pore of Na-montmorillonite with a -0.13 C/m² charge density under different shear rates.

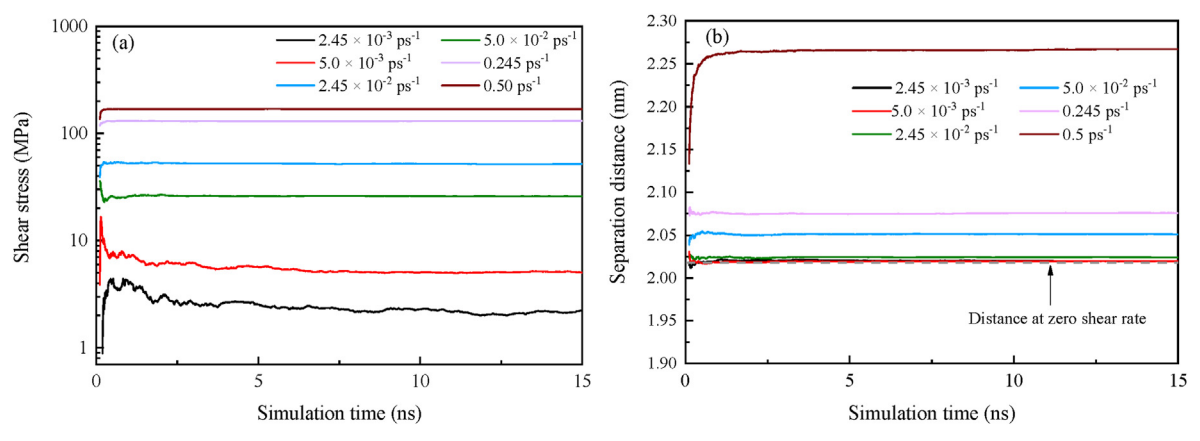


Fig. 8. (a) Shear stress, and (b) separation distance of the Na-montmorillonite model with a -0.13 C/m² charge density under different shear rates with simulation time.

aligns closely with the equilibrium value at zero shear. However, as the shear rate increases, the distance expands, which is consistent with the results of NEMD simulations conducted by Jabbarzadeh and Tanner (2006) on the mica-dodecane system. This expansion is attributed to the destruction of high-speed shear on the structure of the confined water film and its interconnections, such as hydrogen bonds. As a result, the film thickness increases and transitions to lower viscosity values. Nevertheless, this expansion accounts for only a small portion of the overall separation distance and has a minimal impact on the interactions between the two clay plates, as demonstrated in Fig. 9. The profiles of Na⁺ ions within the clay pore at different shear rates exhibit striking similarity, indicating that the shear process has a slight influence on the EDL structure of the clay. Consequently, the interaction between clay particles is considered consistent for a given separation distance under varying shear conditions.

The viscosities at zero shear rate calculated by the Green-Kubo equation from EMD simulations are also plotted. The shear viscosities under different shear rates were obtained from NEMD simulations:

$$\eta = -\frac{\langle p_{yz} \rangle}{\gamma} \tag{9}$$

where p_{yz} is the shear stress in the flow y-direction and the velocity gradient z-direction. The 95% confidence intervals of all the

calculated parameters mentioned above were also estimated by the block-averaged method in this study.

Rheological flow curves of water in 1.1 nm pores of Namontmorillonite with different charge densities are depicted in Fig. 10a. The curve distinctly reveals three regions. At low shear rates $(10^{-7} - 10^{-3} \text{ ps}^{-1})$, the viscosity decreases with increasing shear rate, indicating the shear thinning behavior of montmorillonite. As the shear rate rises $(10^{-3}-10^{-1} \text{ ps}^{-1})$, the curve reaches a plateau where the viscosity closely matches the value calculated by EMD simulation. This plateau signifies the transition of confined water into the Newtonian fluid regime. Subsequently, a second shear-thinning regime is observed at significantly higher shear rates. The whole rheological characteristic is consistent with the generalized viscosity map proposed by Luengo et al. (1996). As a Newtonian fluid, bulk water has a constant viscosity at a low shear rate, where the first shear-thinning regime disappears. However, water still shows bulk shear thinning under ultra high-speed shearing, which has been proven by numerous experiments and simulations (Balasubramanian et al., 1996; Song and Dai, 2010; Kapoor et al., 2014). Therefore, this study primarily focuses on the first two regions of the rheological flow curve, because such extreme high-speed shear conditions are less encountered in engineering practices. Compared to bulk water, the first shearthinning regime demonstrates the non-Newtonian rheological behavior of Na-montmorillonite, which is consistent with experimental findings (e.g. Kök et al., 2000; Wang et al., 2022). The charge

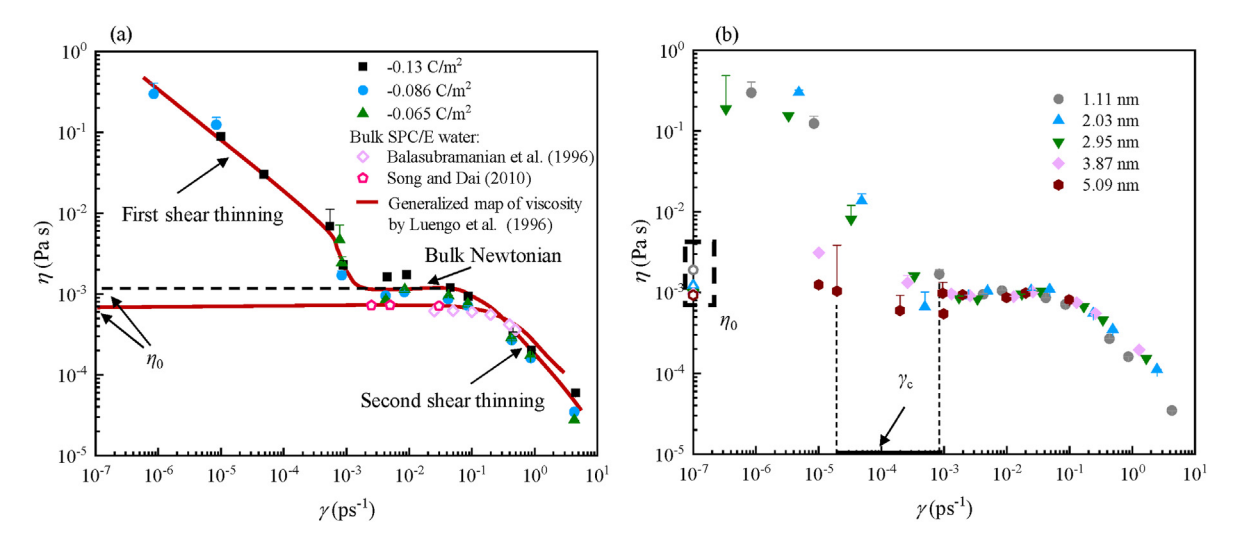


Fig. 10. (a) Viscosity of water molecules in 1.1 nm Na-montmorillonite nanopore with different charge densities and in bulk SPC/E water as a function of the shear rate. The red line represents the generalized map of fluid viscosity under a wide range of shear rates, proposed by Luengo et al. (1996). (b) Water viscosity in Na-montmorillonite pores with different separation distances as a function of the shear rate. The zero shear rate viscosity is shown in the inbox.

density has a minimal influence on the rheological behavior of Namontmorillonite. However, in the bulk Newtonian regime, the viscosity decreases as the charge density decreases, which agrees with the conclusions drawn from EMD simulations.

Water molecules within Na-montmorillonite pores with different separation distances exhibit similar rheological flow curves characterized by three distinct regions, as shown in Fig. 10b. In the first region, the viscosity gradually decreases until it reaches the value calculated by EMD simulations at the zero-shear rate. However, some fluctuations in viscosity are observed within this region. These fluctuations may arise from the slow velocity of the Couette flow at extremely low shear rates, where the background noise generated by the thermal motion of molecules cannot be overlooked. Following the shear thinning behavior, their rheological behavior undergoes a transition from non-Newtonian to Newtonian when the shear rate exceeds the critical shear rate γ_c . By comparing the flow curves at different separation distances, two noteworthy phenomena emerge. First, the viscosity of water in the first region decreases and gradually approaches the value at the zero-shear rate as the separation distance increases. Second, water within larger pores enters the Newtonian region at a lower critical shear rate. Similar phenomena were observed in the micadodecane system simulated by Jabbarzadeh and Tanner (2006). The yield stress can also be estimated using the critical shear rate according to Eq. (9), resulting in values of 2.07 MPa, 0.89 MPa, 0.53 MPa, 0.34 MPa, and 0.19 MPa for separation distances of 1.11-5.09 nm, respectively. This implies that montmorillonite with high water content tends to exhibit Newtonian fluid behavior, characterized by a low yield stress and critical shear rate. The transformation from Newtonian fluid into non-Newtonian behavior for montmorillonite suspensions is also reported as the clay concentration increases (Keren, 1988; Vali and Bachmann, 1988; Shakeel et al., 2021). A similar phenomenon was also found in other clay-water suspensions from experiments, including kaolin, St-Bernard sample, and Eybens clay (Coussot, 1995).

4.2. Yield stress

The yield stress of Na-montmorillonite was determined in the study, and thus the Bingham model was employed. It assumes an ideal material that exhibits plastic flow under a small external shear

stress and transitions into a viscous flow as a Newtonian fluid once the external force exceeds the yield stress. Mathematically, it can be expressed as

$$\tau = \tau_{y} + \mu_{p}\gamma \tag{10}$$

where $\tau_{\rm y}$ is the yield stress and $\mu_{\rm p}$ is the plastic viscosity in the Bingham model.

Fig. 11a shows the diagram of the Bingham model. While the Bingham model may not fit the nonlinear rheological flow curve accurately, it can still be utilized to determine the yield stress (Wang et al., 2023). As illustrated in Fig. 11b, the shear stress of Namontmorillonite exhibits a positive correlation with the shear rate. The yield stress values for each montmorillonite-water system were calculated using Eq. (10), as listed in Table 2. The values are close to those calculated based on the determined critical shear rate. It should be noted that the yield stress obtained in the MD simulation is of orders of magnitude higher than the experimental value, primarily due to the small separation distance between montmorillonite particles. Nevertheless, the magnitude of yield stress is still comparable with particle interactions calculated by the DLVO theory. For the model comprising two parallel Namontmorillonite particles, the yield stress exhibits a good linear relationship with the interaction pressure of the clay particles with R^2 of 97.5%, as depicted in Fig. 12. The simulation results clearly indicate that the yield stress of Na-montmorillonite is directly proportional to the particle interactions, with a scaling factor (approximately 0.5) determined through MD simulation. Previous studies (e.g. Lin et al., 2015; Sakairi et al., 2005; Deng et al., 2023) commonly assumed that the yield stress of clay corresponds to the particle interactions. However, due to the challenges associated with directly measuring the particle interactions of montmorillonite, their relationship has not been examined. Our simulations provide evidence for the existence of a scaling factor between the yield stress and particle interactions in the case of Namontmorillonite. Based on this finding, the yield stress of montmorillonite can be predicted by using DLVO theory (i.e. Eqs. (5), (6) and (8)), which will be discussed in the next section.

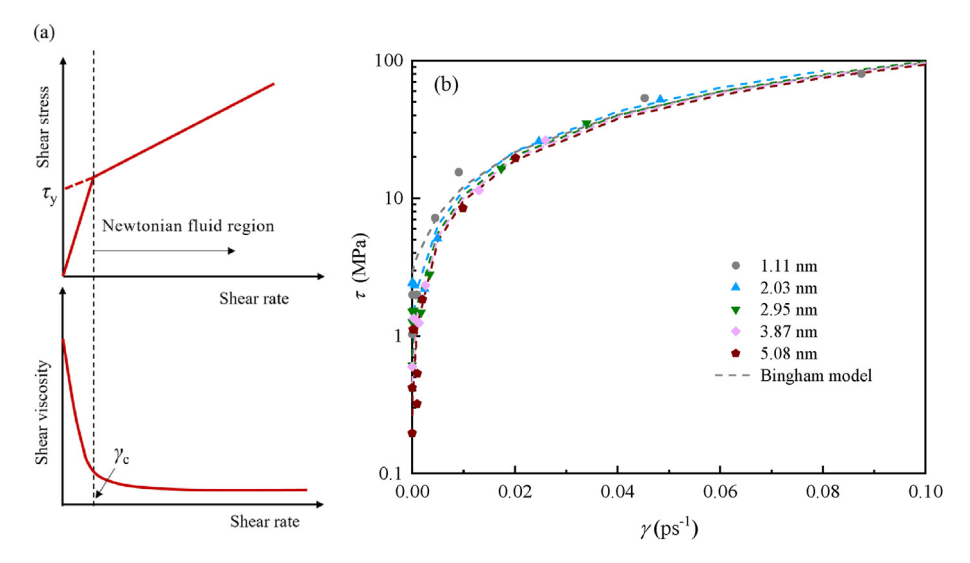


Fig. 11. (a) Diagram of the Bingham model, and (b) Shear stress of Na-montmorillonite with different pore sizes versus shear rate. The simulated data are fitted by the Bingham model.

Table 2The interparticle pressure and yield stress of Na-montmorillonite with different separation distances obtained from MD simulations.

-0.13 C/m ²			-0.086 C/m^2			-0.065 C/m ²		
d (nm)	P (MPa)	τ _y (MPa)	d (nm)	P (MPa)	τ _y (MPa)	d (nm)	P (MPa)	$ au_{ m y}$ (MPa)
1.11	6.16	2.90	1.18	4.63	2.65	1.14	2.93	2.03
2.03	2.19	1.20	2.02	2.08	1.45	2.03	1.68	
2.95	1.17	0.72	3.00	0.72	0.50	2.98	0.56	0.47
3.87	0.64	0.46	3.87	0.52	0.39	3.91	0.42	0.40
5.09	0.48	0.26	5.08	0.36	0.19	5.07	0.34	

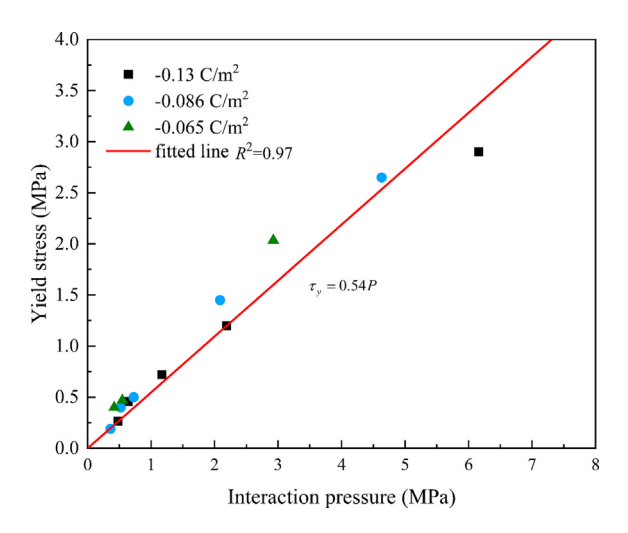


Fig. 12. Relationship between the yield stress and interaction pressure for two parallel Na-montmorillonite particles.

5. Estimation on the yield stress of montmorillonite

5.1. F–F clay structure

Based on the aforementioned MD analysis, this study successfully elucidated the relationship between the yield stress of clay and particle interactions at the nanoscale, as well as the role of particle interactions based on the DLVO theory. Building upon these findings, the model was extended to encompass the macroscopic

rheology of clay suspensions. Initially, the focus was on the clay structure consisting solely of parallel particles, specifically the F–F structure. Bolt (1956) established a relationship between the void ratio and separation distance within such a clay structure:

$$e = \frac{V_{\mathsf{W}}}{V_{\mathsf{c}}} = G_{\mathsf{S}} \rho_{\mathsf{W}} S d = \frac{d}{h} \tag{11}$$

where $V_{\rm w}$ and $V_{\rm s}$ are the volume of water and solids in saturated soil, respectively; $G_{\rm s}$ is the specific gravity of soil particles; $\rho_{\rm w}$ is the water density; S is the specific surface area of soil particles; h is the thickness of particles.

The solid fraction (the mass of clay divided by the whole suspension) is commonly used in clay rheology, which can be expressed as

$$\phi = \frac{V_{\rm S}G_{\rm S}\rho_{\rm W}}{V_{\rm S}G_{\rm S}\rho_{\rm W} + V_{\rm W}\rho_{\rm W}} = \frac{1}{\frac{d}{G_{\rm s}h} + 1}$$
(12)

Taking Eq. (12) into the DLVO theory, the yield stress of clay suspension with different solid fractions can be calculated. Previous studies demonstrated the van der Waals force can be neglected at large separation distances (Laxton and Berg, 2006; Lin et al., 2015). MD simulations in this study (see Fig. 6a) also found that the EDL repulsion plays a major role when d>1 nm. Therefore, the yield stress for an aqueous clay with the F–F structure can be expressed as

$$\tau_{\rm y} = 64a_{\rm f}c^0k_{\rm B}T\tanh^2\left(\frac{\Phi_0}{4}\right)\exp\left[-\kappa G_{\rm s}h\left(\frac{1}{\phi}-1\right)\right] \tag{13}$$

where $a_{\rm f}$ is a scaling factor between yield stress and particle interactions, and ϕ is the solid fraction.

The performance of Eq. (13) should be verified. First, the parameter κ is proportional to the square root of salt concentration based on Eq. (6). Consequently, the relationship between yield stress and electrolyte concentration can be expressed as follows:

$$\tau_{\mathbf{y}} \propto c^0 \exp\left(-\sqrt{c^0}\right) \tag{14}$$

Fig. 13a shows the relationship between yield stress and salt concentration. Abu-Jdayil (2011) measured the yield stress of bentonite with the same solid fraction in different concentrations of electrolyte solutions. The measured yield stress has a good linear relationship with $c^0 \exp(-\sqrt{c^0})$, which is consistent with the prediction of Eq. (14). Second, the temperature effect was considered. Zhang et al. (2022) demonstrated that temperature has little effect on the Debye length (κ^{-1}) over a limited range. Therefore, the yield stress is approximately proportional to the temperature T. Through the comparison with Wyoming Na-bentonite by Vryzas et al. (2017), the relationship between yield stress and temperature is validated, as shown in Fig. 13b.

Finally, the effect of the separation distance (solid fraction) was studied. Fig. 14 presents the yield stress of Na-bentonite with the change of the separation distance in 1×10^{-3} mol/L, 5×10^{-3} mol/L, and 1×10^{-2} mol/L NaCl solutions measured by Sakairi et al. (2005). The distance was calculated by the measured solid fraction based on Eq. (14) by assuming the thickness of the bentonite particle as 0.7 nm. Eq. (13) was also used to estimate the yield stress by taking a scaling factor $a_f = 0.54$ and a surface potential of -90.9 mV as obtained from MD simulations. It shows that the predictions are in good agreement with the tendency to measure values for bentonite in all solutions at a small separation distance. It indicates that the clay particles in the suspension have similar orientations, and the F–F structure plays a major role in the micro-structure of clay when a high solid fraction (small separation distribution) of clay suspension. When the distance exceeds the critical separation distance d_c , Eq. (13) starts to overestimate the yield stress. A low solid fraction suspension forms a loose structure, and the incline angle between particles is greater than zero, leading to a lower particle interaction than the prediction by Eq. (13) under the parallel plate assumption. In addition, the predictions are larger than the measurements for bentonite in 1×10^{-3} mol/L and 5×10^{-3} mol/L NaCl solutions. The reason may be attributed to the change in scaling factor and surface potential for different salt concentrations. In

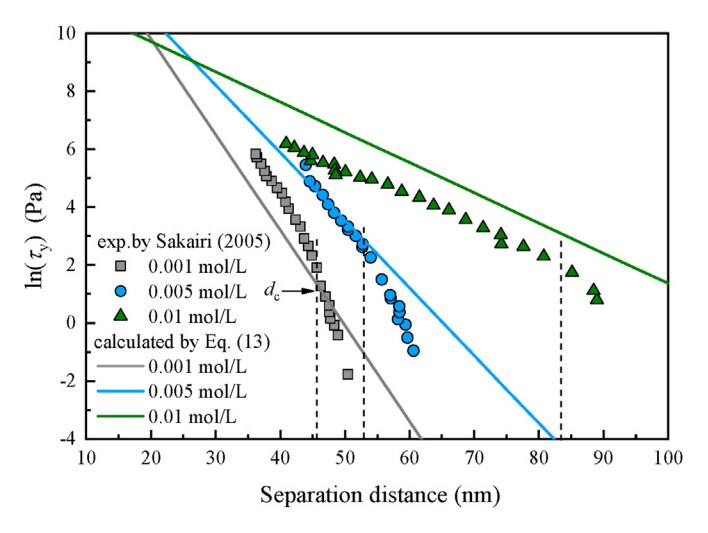


Fig. 14. Relationship between the yield stress and separation distance for bentonite suspensions in different concentrations of NaCl solutions calculated by Eq. (13), compared with experimental data measured by Sakairi et al. (2005).

other words, the proposed equation demonstrates satisfactory performance in predicting the yield stress of bentonite suspensions under the influence of factors, including electrolyte concentration, temperature, and separation distance (solid fraction). However, it should be noted that the proposed equation tends to overestimate the yield stress in low solid fraction suspensions, where the presence of non-parallel plates in the clay structure should be taken into consideration.

5.2. Yield stress for non-parallel plates

The microstructure of clay was further investigated by examining the variations in separation distance d and incline angle α . For simplicity, a uniform clay structure was considered, where there is the same d and α between particles with the same size of $l \times h$. The minimum representative elementary volume (REV) is depicted in Fig. 15. In the REV, two half particles are positioned at the top and bottom, as the remaining half particles are shared with other REVs. Additionally, a particle is situated in the middle of the REV, featuring an incline angle α . The minimum distance between particles is denoted as d_{\min} . Consequently, the solid fraction can be expressed as

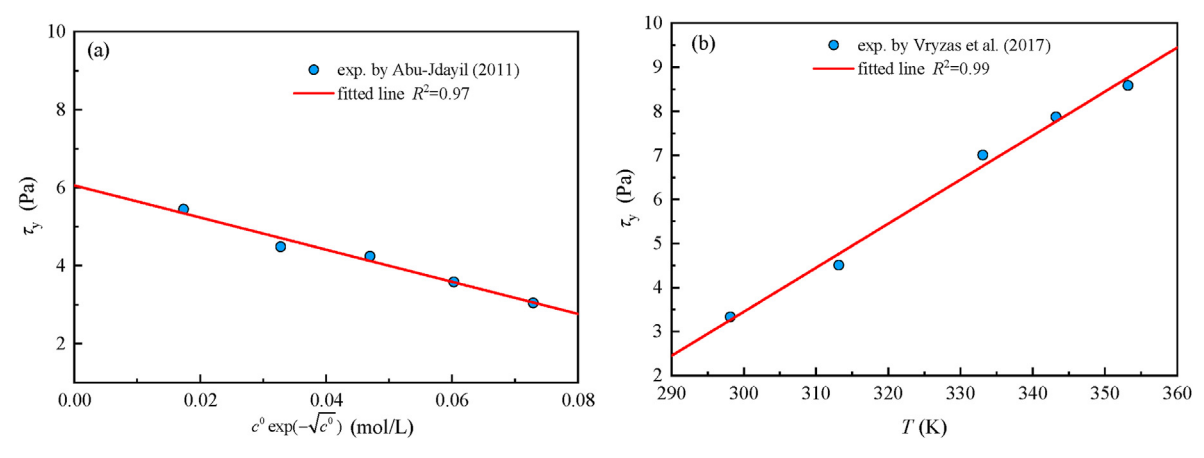


Fig. 13. Relationship between the yield stress of bentonite suspension and (a) electrolyte concentration, and (b) temperature.

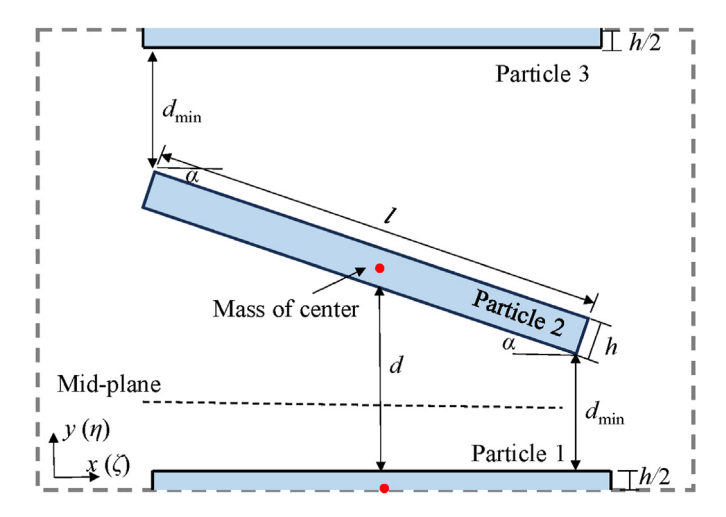


Fig. 15. Diagram of representative elementary volume for non-parallel particles.

$$\phi = \frac{2hlG_{s}\rho_{w}}{2hlG_{s}\rho_{w} + 2d_{\min}l\rho_{w} + l^{2}\sin\alpha\rho_{w}} = \frac{1}{1 + \frac{d_{\min} + 0.5l\sin\alpha}{hG_{s}}}$$
(15)

The separation distance between two particles takes the distance between the centers of mass for two particles minus the thickness of the particle, namely $d=d_{\min}+0.5l\sin\alpha$. Taking this into Eq. (15), we then have Eq. (13), implying the relationship between solid fraction and separation distribution is unchanged with incline angles. However, the interaction between two particles depends on the projected area of the particle on the mid-plane. Thus, the yield stress for non-parallel clay particles should be written as follows:

$$\tau_{\rm y} = 64a_{\rm f}c^0k_{\rm B}T\cos\alpha\tanh^2\left(\frac{\Phi_0}{4}\right)\exp\left[-\kappa hG_{\rm S}\left(\frac{1}{\phi}-1\right)\right] \tag{16}$$

Previous models for predicting the yield stress of clay suspensions have incorporated the influence of non-particle particle structure (e.g. Lin et al., 2015; Deng et al., 2023). However, limited research has focused on the evolution of clay structure in relation to

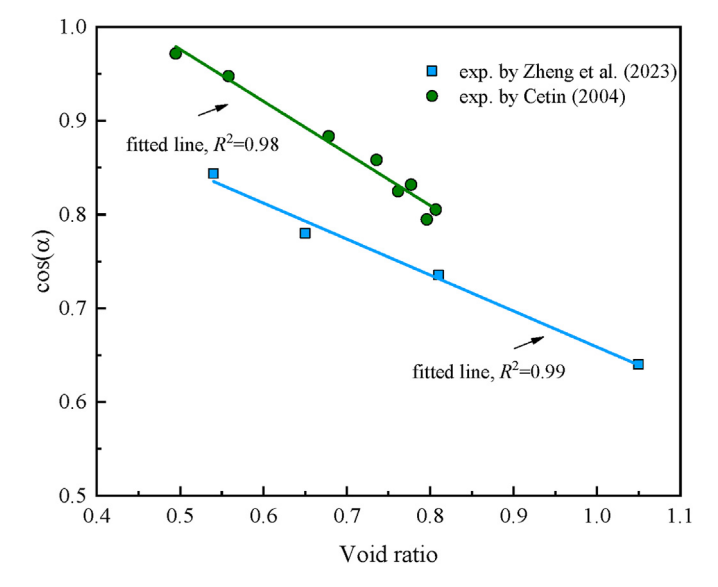


Fig. 16. Evolution of averaged incline angle between particles as a function of void ratio measured by Cetin (2004) and Zheng et al. (2022).

changes in solid fractions. Cetin (2004) measured the average angles of particle orientations during the consolidation of cohesive soils, while Zheng et al. (2022) analyzed the pore orientation distribution during the consolidation of an illitic clay using SEM. In this study, the average incline angle as a function of void ratio is compiled, as illustrated in Fig. 16. The incline angle value decreases linearly with increasing void ratio for both soils. Based on Eq. (11), it can be observed that the separation distance exhibits a linear relationship with the void ratio. Consequently, a function involving the solid fraction and the cosine of the incline angle is derived as follows:

$$\cos \alpha = -\frac{a}{\phi} + b \quad (\phi < \phi_{c})$$

$$\cos \alpha = 1 \quad (\phi \ge \phi_{c})$$
(17)

where a and b are the two fitting parameters; $\phi_{\rm c} = a/(b-1)$ is the critical solid fraction, which the incline angle changes with solid fraction when smaller than the critical value and becomes zero when greater than $\phi_{\rm c}$.

Finally, the yield stress of the clay suspension can be determined by combining Eqs. (16) and (17). To facilitate usability, the scaling factor and surface potential in Eq. (16) are assigned values obtained from MD simulations. The specific gravity of the clay particle is assumed to be 2.65. Therefore, when calculating the yield stress, it is necessary to fit the incline angle between particles, the average thickness of the particle, and the electrolyte concentration (if not provided). The estimated yield stress (in Pa) of the clay suspension at room temperature (300 K) is as follows:

$$ln(\tau_y) = 18.5 + ln(c^0) + ln(\cos\alpha) - 8.7h\sqrt{c^0}\left(\frac{1}{\phi} - 1\right)$$
 (18)

The incline angle α can be fitted by Eq. (18). According to Eq. (18), the yield stress is dependent on the electrolyte concentration, thickness and incline angle of clay particles, and solid fraction of bentonite suspension. Fig. 17a and b presents the predicted yield stress as a function of solid fraction based on Eq. (18), compared with measured data in previous literature. The fitted parameters are listed in Table 3. The proposed model exhibits good performance in predicting the yield stress of bentonite suspensions. The fitted electrolyte concentrations match with the values reported in the literature (e.g. Sakairi et al., 2005), indicating the high accuracy of the proposed model. As shown in Table 3, the average thickness of clay particles has a great influence on the $\tau_{\rm y}$ – ϕ relationship. Furthermore, the change in incline angle is observed only in the bentonite sample with high concentrations of solutions. The critical solid fraction ϕ_c decreases with an increase in the electrolyte concentration. This can be attributed to the reduction in the extent of the EDL repulsive force with increasing electrolyte concentration, leading to a tendency for clay particles to become disordered under the same separation distribution. The value of the scaling factor is deemed appropriate after comparing the estimation values obtained from our proposed model with experimental results. It should be noted that the specific value of the scaling factor is not of utmost importance since the concentration and particle thickness need to be adjusted when estimating the yield stress of clay. Nevertheless, this paper emphasizes the existence of the scaling factor as a representation of the difference between yield stress and particle interactions. In summary, the proposed model combines the DLVO theory with the microstructure of the clay suspension, and it demonstrates satisfactory performance in predicting the yield stress of bentonite suspensions.

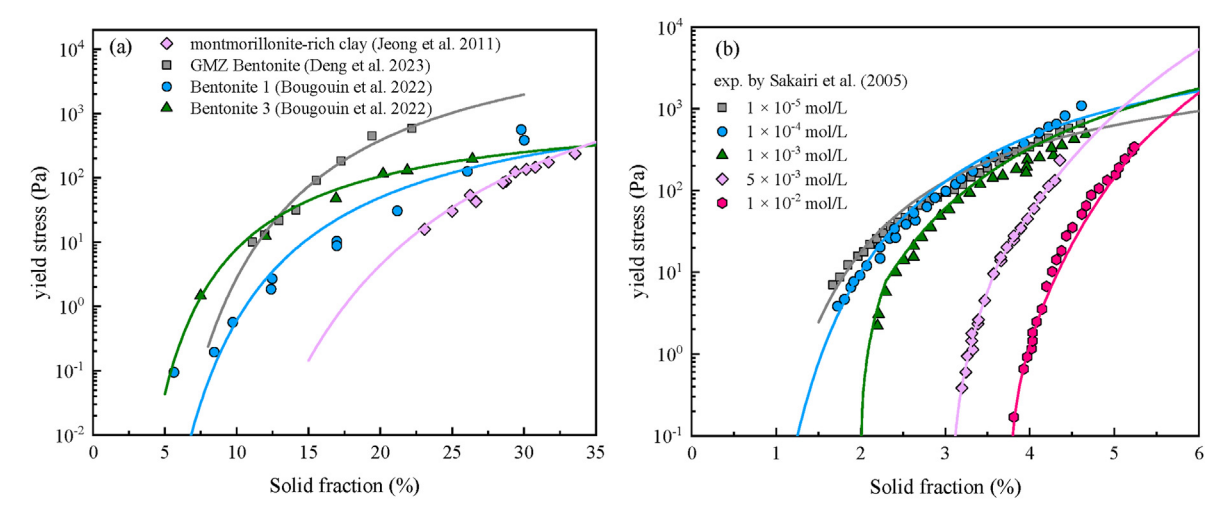


Fig. 17. Predicted yield stress of bentonite suspensions as a function of solid fraction based on Eqs. (17) and (18), compared with published experimental data.

Table 3Fitted parameters in the proposed model for predicting the yield stress of bentonite suspensions.

Clay	Immersed solution	c ⁰ (mol/L)	h (nm)	а	φ _c (%)	Source
Montmorillonite-rich clay	water	1×10^{-4}	20.1		0	Jeong et al. (2012)
GMZ bentonite	water	2×10^{-4}	8.3		0	Deng et al. (2023)
Bentonite 1	water	1×10^{-5}	27.0		0	Bougouin et al. (2022)
Bentonite 3	water	8×10^{-6}	22.5		0	
Na-bentonite	1×10^{-5} mol/L NaCl	$5 imes 10^{-5}$	1.9		0	Sakairi et al. (2005)
	1×10^{-4} mol/L NaCl	$1.4 imes 10^{-4}$	1.4		0	
	1×10^{-3} mol/L NaCl	3×10^{-4}	1.2	-0.14	2.5	
	5×10^{-3} mol/L NaCl	2×10^{-2}	0.6	-0.20	3.6	
	1×10^{-2} mol/L NaCl	$4 imes 10^{-2}$	0.6	-0.13	5.0	

6. Conclusions

In this paper, the rheological behaviors of Na-montmorillonite were investigated based on equilibrium and non-equilibrium molecule dynamics. Particularly, the study emphasized the relationship between rheology and interparticle interactions. According to MD simulations, a model was proposed to estimate the yield stress of montmorillonite based on the DLVO theory and the incline angle between clay particles. The main conclusions can be summarized as follows:

- (1) In the MD simulation, the viscosity of water confined in Namontmorillonite pores increased exponentially with decreasing pore size. It was observed that the classical DLVO theory underestimates the interactions when the separation distance between particles is small. A fitting equation was employed to better predict the interaction pressure across varying separation distances. The surface charge density of clay particles had a minimal effect on water viscosity and particle interactions, which became even more negligible as the separation distance increased significantly.
- (2) The MD results showed that Na-montmorillonite with different water content exhibited typical shear thinning behaviors across a wide range of shear rates. However, as the water content increased, the rheological behavior of montmorillonite approached that of Newtonian fluids, characterized by low yield stress and critical shear stress. The yield stress of Na-montmorillonite was determined, revealing a linear relationship between the particle interaction and yield stress.

(3) Based on the MD results, a comprehensive model was developed to estimate the yield stress of montmorillonite. This model considered the strength of particle interaction between two non-parallel plates. Through comparison with experimental data, the proposed model demonstrated excellent performance in predicting the yield stress of bentonite under various influencing factors, including electrolyte concentration, temperature, and solid fraction.

CRediT authorship contribution statement

Siqi Zhang: Writing — original draft, Software, Methodology, Investigation. **Daoyuan Tan:** Writing — review & editing, Funding acquisition, Conceptualization. **Honghu Zhu:** Writing — review & editing, Supervision. **Huafu Pei:** Writing — review & editing, Funding acquisition, Formal analysis. **Bin Shi:** Writing — review & editing, Supervision, Conceptualization.

Declaration of competing interest

The authors declare that they have no known competing financial interests or personal relationships that could have appeared to influence the work reported in this paper.

Acknowledgments

The authors gratefully acknowledge the financial support provided by the National Science Fund for Distinguished Young Scholars of China (Grant No. 42225702), the National Natural Science Fund of China for Excellent Young Scholars Fund (Overseas),

Applied Basic Research Programme of Liaoning Province (2023JH2/101300139), Opening fund of State Key Laboratory of Geohazard Prevention and Geoenvironment Protection (Chengdu University of Technology, SKLGP2024K020), and Key Laboratory of Earth Fissures Geological Disaster, Ministry of Natural Resources.

References

- Abdurrahmanoglu, S., Okay, O., 2010. Rheological behavior of polymer—clay nanocomposite hydrogels: effect of nanoscale interactions. J. Appl. Polym. Sci. 116, 2658—2667. https://doi.org/10.1002/app.
- Abraham, M.T., Satyam, N., Pradhan, B., Tian, H., 2022. Debris flow simulation 2D (DFS 2D): numerical modelling of debris flows and calibration of friction parameters. J. Rock Mech. Geotech. Eng. 14 (6), 1747–1760.
- Abu-Jdayil, B., 2011. Rheology of sodium and calcium bentonite—water dispersions: Effect of electrolytes and aging time. Int. J. Miner. Process 98 (3-4), 208–213.
- Amarasinghe, P.M., Anandarajah, A., 2013. Molecular dynamic study of the swelling behavior of Na-montmorillonite. Environ. Eng. Geosci. 19 (2), 173–183.
- Anandarajah, A., Amarasinghe, P.M., 2013. Discrete-element study of the swelling behaviour of Na-montmorillonite. Geotechnique 63 (8), 674–681.
- Avery, R.G., Ramsay, J.D.F., 1986. Colloidal properties of synthetic hectorite clay dispersions. II. Light and small angle neutron scattering. J. Colloid Interface Sci. 109, 448–454.
- Balasubramanian, S., Mundy, C.J., Klein, M.L., 1996. Shear viscosity of polar fluids: molecular dynamics calculations of water. J. Chem. Phys. 105, 11190—11195.
- Benna, M., Kbir-Ariguib, N., Magnin, A., Bergaya, F., 1999. Effect of pH on rheological properties of purified Sodium bentonite suspensions. J. Colloid Interface Sci. 218, 442–455.
- Bolt, G.H., 1956. Physico-chemical analysis of the compressibility of pure clays. Geotechnique 6 (2), 86–93.
- Bougouin, A., Pantet, A., Ahfir, N.D., 2022. Quantifying the yield stress of bentonite muds mixed with other clays during drilling operations. Appl. Clay Sci. 228, 106593.
- Bourg, I.C., Sposito, G., 2011. Molecular dynamics simulations of the electrical double layer on smectite surfaces contacting concentrated mixed electrolyte (NaCl–CaCl₂) solutions. J. Colloid Interface Sci. 360 (2), 701–715.
- Brandenburg, U., Lagaly, G., 1988. Rheological properties of sodium montmorillonite dispersions. Appl. Clay Sci. 3, 263–279.
- Cetin, H., 2004. Soil-particle and pore orientations during consolidation of cohesive soils. Eng. Geol. 73 (1–2), 1–11.
- Chegbeleh, L.P., Yidana, S.M., Nishigaki, M., Achampong, F., 2014. Comparative study on the application of ethanol-bentonite slurry and salt-bentonite slurry as effective injection materials for barrier sealing. Appl. Clay Sci. 87, 40–45.
- Coussot, P., 1995. Structural similarity and transition from Newtonian to non-Newtonian behavior for clay-water suspensions. Phys. Rev. Lett. 74, 3971–3974.
- Cygan, R.T., Liang, J.J., Kalinichev, A.G., 2004. Molecular models of hydroxide, oxyhydroxide, and clay phases and the development of a general force field. J. Phys. Chem. B 108, 1255–1266.
- Deng, R., Chen, B., Liu, C., 2023. Concentration dependence of yield stress of bentonite suspension and corresponding particle interactions. Comput. Geotech. 157, 105358.
- Dickinson, E., 2013. Structure and rheology of colloidal particle gels: insight from computer simulation. Adv. Colloid Interface Sci. 199, 114–127.
- Du, M., Liu, P., Wong, J.E., Clode, P.L., Liu, J., Leong, Y.K., 2020. Colloidal forces, microstructure and thixotropy of sodium montmorillonite (SWy-2) gels: Roles of electrostatic and van der Waals forces. Appl. Clay Sci. 195, 105710.
- Du, J., Zhou, A., Lin, X., Robert, D., Giustozzi, F., Kodikara, J., 2023. Modeling microstructural mechanical behavior of expansive soil at various water contents and dry densities by molecular dynamics simulation. Comput. Geotech. 158, 105371.
- Durán, J.D.G., Ramos-Tejada, M.M., Arroyo, F.J., González-Caballero, F., 2000. Rheological and electrokinetic properties of sodium montmorillonite suspensions. J. Colloid Interface Sci. 229, 107–117.
- Feng, W.Q., Yin, J.H., Tao, X.M., Tong, F., Chen, W.B., 2017. Time and strain-rate effects on viscous stress—strain behavior of plasticine material. Int. J. GeoMech. 17 (5), 04016115
- Gijven, N., 1990. Longevity of bentonite as buffer material in a nuclear-waste repository. Eng. Geol. 28, 233–247.
- Günister, E., Işçi, S., Öztekin, N., Erim, F.B., Ece, Ö.I., Güngör, N., 2006. Effect of cationic surfactant adsorption on the rheological and surface properties of bentonite dispersions. J. Colloid Interface Sci. 303, 137–141.
- Gupta, V., Hampton, M.A., Stokes, J.R., Nguyen, A.V., Miller, J.D., 2011. Particle interactions in kaolinite suspensions and corresponding aggregate structures. J. Colloid Interface Sci. 303 (359), 95–103, 1.
- Hattab, M., Hammad, T., Fleureau, J.M., 2015. Internal friction angle variation in a kaolin/montmorillonite clay mix and microstructural identification. Geotechnique 65 (1), 1–11.
- Heimenz, P.C., 1986. Principles of Colloid and Surface Chemistry. M. Dekker, New York
- Holmboe, M., Bourg, I.C., 2014. Molecular dynamics simulations of water and sodium diffusion in smectite interlayer nanopores as a function of pore size and temperature. J. Phys. Chem. C 118, 1001–1013.

- Hou, J., Li, H., Zhu, H., Wu, L., 2009. Determination of clay surface potential: a more reliable approach. Soil Sci. Soc. Am. J. 73 (5), 1658–1663.
- Hsiao, Y.W., Hedstrom, M., 2017. Swelling pressure in systems with Namontmorillonite and neutral surfaces: a molecular dynamics study. J. Phys. Chem. C 121 (47), 26414–26423.
- Jabbarzadeh, A., Tanner, R.I., 2006. Molecular dynamics simulation and its application to nano-rheology. Rheol. Rev 165.
- Jabbarzadeh, A., Atkinson, J.D., Tanner, R.I., 1997. Rheological properties of thin liquid films by molecular dynamics simulations. J. Nonnewton. Fluid Mech (69), 169–193.
- Jeong, S.W., Locat, J., Leroueil, S., 2012. The effects of salinity and shear history on the rheological characteristics of illite-rich and Na-montmorillonite-rich clays. Clays Clay Miner. 60 (2), 108–120.
 Kapoor, K., Amandeep, Patil, S., 2014. Viscoelasticity and shear thinning of nano-
- Kapoor, K., Amandeep, Patil, S., 2014. Viscoelasticity and shear thinning of nanoconfined water. Phys. Rev. E Stat. Nonlinear Soft Matter Phys. 89, 1–7.
 Katti, D.R., Thapa, K.B., Katti, K.S., 2018. The role of fluid polarity in the swelling of
- Katti, D.R., Thapa, K.B., Katti, K.S., 2018. The role of fluid polarity in the swelling of sodium-montmorillonite clay: a molecular dynamics and Fourier transform infrared spectroscopy study. × × J Rock Mech. Geotech. Eng. 10 (6), 1133–1144.
- Keren, R., 1988. Rheology of aqueous suspension of sodium/calcium montmorillonite. Soil Sci. Soc. Am. J. 52, 924–928.
- Kök, M.V., Batmaz, T., Gücüyener, I.H., 2000. Rheological behavior of bentonite suspensions. Petrol. Sci. Technol. 18, 519–536.
- Komine, H., Ogata, N., 2004. Predicting swelling characteristics of bentonites. J. Geotech. Geoenviron. Eng. 130 (8), 818–829.
- Kröger, M., Hess, S., 2000. Rheological evidence for a dynamical crossover in polymer melts via nonequilibrium molecular dynamics. Phys. Rev. Lett. 85, 1128–1131
- Kyokawa, H., 2021. A double structure model for hydro-mechano-chemical behavior of expansive soils based on the surface phenomena of mineral crystals. Eng. Geol. 294, 106366.
- Landrou, G., Brumaud, C., Plötze, M.L., Winnefeld, F., Habert, G., 2018. A fresh look at dense clay paste: deflocculation and thixotropy mechanisms. Colloids Surfaces A Physicochem. Eng. Asp. 539, 252–260.
- Laribi, S., Fleureau, J.M., Grossiord, J.L., Kbir-Ariguib, N., 2005. Comparative yield stress determination for pure and interstratified smectite clays. Rheol. Acta 44, 262–269.
- Laxton, P.B., Berg, J.C., 2006. Relating clay yield stress to colloidal parameters. J. Colloid Interface Sci. 296, 749–755.
- Lee, J.H., Guggenheim, S., 1981. Single crystal X-ray refinement of pyrophyllite-1 Tc. Am. Mineral. 66, 350–357.
- Leong, Y.K., 2024. Direct evidence of electric double layer (EDL) repulsive force being responsible for the time-dependent behavior of clay gels in the structural rejuvenation mode. J. Phys. Chem. B 128 (15), 3784–3793.
- Li, Y., Narayanan Nair, A.K., Kadoura, A., Yang, Y., Sun, S., 2019. Molecular simulation study of montmorillonite in contact with water. Ind. Eng. Chem. Res. 58, 1396–1403.
- Li, B., Li, C., Gui, Y., Zhan, H., Gu, Y., Yu, M., Rowe, R.K., 2024. Understanding structural anisotropy and mechanical properties of Na-montmorillonite with crystalline swelling and uniaxial deformation under different hydration degrees. Comput. Geotech. 169, 106200.
- Liingaard, M., Augustesen, A., Lade, P.V., 2004. Characterization of models for time-dependent behavior of soils. Int. J. GeoMech. 4 (3), 157–177.
- Lin, Y., Phan-Thien, N., Lee, J.B.P., Khoo, B.C., 2015. Concentration dependence of yield stress and dynamic moduli of kaolinite suspensions. Langmuir 31 (16), 4791–4797.
- Liu, X., Feng, B., Tian, R., Li, R., Tang, Y., Wu, L., Ding, W., Li, H., 2020. Electrical double layer interactions between soil colloidal particles: polarization of water molecule and counterion. Geoderma 380, 114693.
- Low, P.F., 1976. Viscosity of interlayer water in montmorillonite. Soil Sci. Soc. Am. J. 40, 500–505.
- Low, P.F., 1980. The swelling of clay: II. Montmorillonites. Soil Sci. Soc. Am. J. 44 (4), 667–676.
- Luckham, P.F., Rossi, S., 1999. Colloidal and rheological properties of bentonite suspensions. Adv. Colloid Interface Sci. 82, 43—92.
- Luengo, G., Israelachvili, J., Granick, S., 1996. Generalized effects in confined fluids: new friction map for boundary lubrication. Wear 200 (1–2), 328–335. Mark, P., Nilsson, L., 2001. Structure and dynamics of the TIP3P, SPC, and SPC/E
- water models at 298 K. J. Phys. Chem. A 105, 9954–9960.
 Martínez, L., Andrade, R., Birgin, E.G., Martínez, J.M., 2009. PACKMOL: a package for
- Martínez, L., Andrade, R., Birgin, E.G., Martínez, J.M., 2009. PACKMOL: a package for building initial configurations for molecular dynamics simulations. J. Comput. Chem. 30 (13), 2157–2164.
- Meng, J., Li, C., Zhou, J.Q., Zhang, Z., Yan, S., Zhang, Y., Huang, D., Wang, G., 2023. Multiscale evolution mechanism of sandstone under wet-dry cycles of deionized water: from molecular scale to macroscopic scale. \times \times J Rock Mech. Geotech. Eng. 15 (5), 1171–1185.
- Neuzil, C.E., 2019. Permeability of clays and shales. Annu. Rev. Earth Planet Sci. 47, 247–273.
- Pei, H., Zhang, S., 2021. Molecular dynamics study on the zeta potential and shear plane of montmorillonite in NaCl solutions. Appl. Clay Sci. 212, 106212.
- Pisarev, V.V., Kalinichev, A.G., 2022. Couette flow of pentane in clay nanopores: molecular dynamics simulation. J. Mol. Liq. 366, 120290.
- Plimpton, S., 1995. Fast parallel algorithms for short-range molecular dynamics. J. Comput. Phys. 117 (1), 1–19.
- Ramos-Tejada, M.M., Arroyo, F.J., Perea, R., Durán, J.D.G., 2001. Scaling behavior of the rheological properties of montmorillonite suspensions: correlation between

- interparticle interaction and degree of flocculation. J. Colloid Interface Sci. 235, 251–259
- Ren, J., Deshun, Y., Zhai, R., 2021. Rheological behavior of bentonite-water suspension at various temperatures: effect of solution salinity. Eng. Geol. 295, 106435.
- Sakairi, N., Kobayashi, M., Adachi, Y., 2005. Effects of salt concentration on the yield stress of sodium montmorillonite suspension. J. Colloid Interface Sci. 283 (1), 245–250.
- Salih, A., 2022. Multiscale approaches including ANN and M5P-tree with SI and OBJ assessment tools to predict the shear thinning of bentonite drilling muds modified with clay nanosize at various elevated temperatures. Int. J. GeoMech. 22 (1). 04021246.
- Shakeel, A., Kirichek, A., Chassagne, C., 2021. Rheology and yielding transitions in mixed kaolinite/bentonite suspensions. Appl. Clay Sci. 211, 106206.
- Shen, X., Bourg, I.C., 2021. Molecular dynamics simulations of the colloidal interaction between smectite clay nanoparticles in liquid water. J. Colloid Interface Sci. 584, 610–621.
- Song, Y., Dai, L.L., 2010. The shear viscosities of common water models by non-equilibrium molecular dynamics simulations. Mol. Simulat. 36 (7–8), 560–567. Sridharan, A., Choudhury, D., 2002. Swelling pressure of sodium montmorillonites. Geotechnique 52 (6), 459–462.
- Sridharan, A., Jayadeva, M.S., 1982. Double layer theory and compressibility of clays. Geotechnique 32 (2), 133–144.
- Teh, E.J., Leong, Y.K., Liu, Y., Fourie, A.B., Fahey, M., 2009. Differences in the rheology and surface chemistry of kaolin clay slurries: the source of the variations. Chem. Eng. Sci. 64 (17), 3817–3825.
- Vali, H., Bachmann, L., 1988. Ultrastructure and flow behavior of colloidal smectite dispersions. J. Colloid Interface Sci. 126, 278–291.
- Vryzas, Z., Kelessidis, V.C., Nalbantian, L., Zaspalis, V., Gerogiorgis, D.I., Wubulikasimu, Y., 2017. Effect of temperature on the rheological properties of neat aqueous Wyoming sodium bentonite dispersions. Appl. Clay Sci. 136, 26–36
- Wang, Z., Ding, W., Zhu, Z., Liu, R., Wang, C., Yu, W., Wang, Z., 2022. Experimental study on rheological behaviors of Na-bentonite slurries under seawater intrusion. Construct. Build. Mater. 357, 129369.
- Wang, Z., Guo, W., Ding, W., Liu, K., Qin, W., Wang, C., Wang, Z., 2023. Numerical study on the hydrodynamic properties of bentonite slurries with Herschel-Bulkley-Papanastasiou rheology model. Powder Technol. 419, 118375.
- Wei, P., Zheng, Y.Y., Xiong, Y., Zhou, S., Al-Zaoari, K., Zaoui, A., 2022. Effect of water content and structural anisotropy on tensile mechanical properties of montmorillonite using molecular dynamics. Appl. Clay Sci. 228, 106622.
- Wei, P., Zhou, S., Zheng, Y.Y., Yin, Z.Y., Xu, W., 2024. Nanoscale stick-slip behavior and hydration of hydrated illite clay. Comput. Geotech. 166, 105976.
- Xie, Y., Hou, M.Z., Liu, H., Li, C., 2023. Anisotropic time-dependent behaviors of shale under direct shearing and associated empirical creep models. × × J Rock Mech. Geotech. Eng. 16 (4), 1262–1279.
- Xu, D., Bhatnagar, D., Gersappe, D., Sokolov, J.C., Rafailovich, M.H., Lombardi, J., 2015. Rheology of poly (N-isopropylacrylamide)—clay nanocomposite hydrogels. Macromolecules 48 (3), 840–846.
- Xu, W.Q., Yin, Z.Y., Zheng, Y.Y., 2023. Investigating silica interface rate-dependent friction behavior under dry and lubricated conditions with molecular dynamics. Acta Geotech 18 (7), 3543–3554.
- Yan, H., Zhang, Z., 2021. Effect and mechanism of cation species on the gel

- properties of montmorillonite. Colloids Surfaces A Physicochem. Eng. Asp. 611, 125824.
- Yeh, I.C., Hummer, G., 2004. System-size dependence of diffusion coefficients and viscosities from molecular dynamics simulations with periodic boundary conditions. J. Phys. Chem. B 108, 15873—15879.
- Ying, H.C., Pei, H.F., Zhang, S.Q., 2024. Investigation on the friction properties of montmorillonite by molecular dynamics considering the effects of water content, cation species, ion concentration and temperature. Comput. Geotech. 171, 106345
- Yoon, J., El Mohtar, C.S., 2015. A filtration model for evaluating maximum penetration distance of bentonite grout through granular soils. Comput. Geotech. 65, 291–201
- Yoshida, T., Tasaka, Y., Tanaka, S., Park, H.J., Murai, Y., 2018. Rheological properties of montmorillonite dispersions in dilute NaCl concentration investigated by ultrasonic spinning rheometry. Appl. Clay Sci. 161, 513—523.
- Yoshida, T., Tasaka, Y., Fischer, P., Murai, Y., 2022. Time-dependent viscoelastic characteristics of montmorillonite dispersion examined by ultrasonic spinning rheometry. Appl. Clay Sci. 217, 106395. https://doi.org/10.1016/ j.clay.2021.106395.
- Zhang, C., Lu, N., 2018. What is the range of soil water density? critical reviews with a unified model. Rev. Geophys. 56 (3), 532–562.
- Zhang, S., Pei, H., 2021. Determining the bound water content of montmorillonite from molecular simulations. Eng. Geol. 294, 106353.Zhang, S., Pei, H., Plötze, M., Ying, H., 2022. Molecular dynamics modeling of hy-
- Zhang, S., Pei, H., Plötze, M., Ying, H., 2022. Molecular dynamics modeling of hydraulic conductivity of soil considering variable viscosity and adsorbed water. Appl. Clay Sci. 228.
- Zhao, S., Wang, F.Y., Tan, D.Y., Yang, A.W., 2024. A deep learning informed-mesoscale cohesive numerical model for investigating the mechanical behavior of shield tunnels with crack damage. Structures 66, 106902.
- Zheng, Y., Baudet, B.A., Delage, P., Pereira, J.M., Sammonds, P., 2022. Pore changes in an illitic clay during one-dimensional compression. Geotechnique 73 (10), 917–932.



Dr. Daoyuan Tan is an Associate Professor at School of Earth Sciences and Engineering, Nanjing University. He obtained his Bachelor's and Master's degrees from the China University of Geosciences and his PhD from the Hong Kong Polytechnic University, respectively. His areas of research interests include geohazards management, intelligent monitoring of geotechnical structures and development of smart city infrastructure. He has been the Principal Investigator leading one General Research Fund by the Hong Kong Research Grants Council and the Excellent Young Scientists Fund (Overseas) by the National Natural Science Foundation of China (NSFC). He currently serves as the nominated committee member of TC220, Field Monitoring in Geomechanics, International

Society for Soil Mechanics and Geotechnical Engineering (ISSMGE). He was awarded the Ringo Yu Prize for Best PhD Thesis in Geotechnical Studies from The Hong Kong Institution of Engineers (HKIE) in 2020 and the Fugro Prize (1st Runner-up) in 2023.